JBIC Journal of Biological Inorganic Chemistry (2019) 24:365–376
https://doi.org/10.1007/s00775-019-01653-6

ORIGINAL PAPER

Structural analysis and biological functionalities of iron(III)– and manganese(III)–thiosemicarbazone complexes: in vitro anti-proliferative activity on human cancer cells, DNA binding and cleavage studies

Büşra Kaya[1] · Zehra Kübra Yılmaz[2] · Onur Şahin[3] · Belma Aslim[2] · Ümmügülsüm Tükenmez[4] · Bahri Ülküseven[1]

Received: 21 January 2019 / Accepted: 13 March 2019 / Published online: 20 March 2019

Abstract

One iron(III) and two manganese(III) complexes based on thiosemicarbazone were synthesized and characterized using analytical and spectroscopic data. The crystallographic analysis showed the square pyramid structures of the complexes. Electronic spectra analysis was performed to determine the nature of the interaction between the complexes and calf thymus DNA (CT-DNA). DNA cleavage activities of the complexes were examined by gel electrophoresis (pBR322 DNA). The cytotoxicity of the complexes was determined against human cervical carcinoma (HeLa) and human colorectal adenocarcinoma (HT-29) cell lines by MTT assay. The results indicated that complex Fe1 is bound to CT-DNA via the intercalation mode, while complexes Mn1 and Mn2 are bound to CT-DNA via groove binding and/or electrostatic interactions rather than the intercalation mode. In addition, they showed good binding activity, which followed the order of Fe1 > Mn2 > Mn1. Complexes were found to promote the cleavage of DNA from supercoiled form (SC, Form I) to nicked circular form (NC, Form II) without concurrent formation of Form III, revealing the single-strand DNA cleavage. No significant cleavage was found in the presence of Mn1 and Mn2; however, it was observed at 2000 and 3000 μM concentrations of Fe1. The ability of Fe1 to cleave DNA was greater than that of other complexes and these results are in conformity with their DNA-binding affinities. Cytotoxicity determination tests revealed that the complex Fe1 on HeLa and HT-29 cells exhibited a higher anti-proliferative effect than Mn1 and Mn2 (Fe1 > Mn2 > Mn1). These studies suggested that the complex Fe1 could be a good candidate as a chemotherapeutic drug targeting DNA.

Graphical abstract

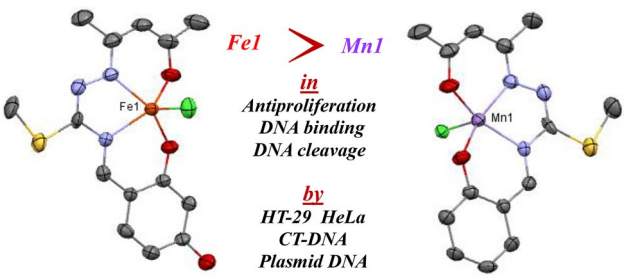

Keywords Thiosemicarbazone · Iron · Manganese · DNA binding · DNA cleavage · Anti-proliferation

Introduction

Biologically functional molecules are one of the top preferential topics in chemistry research. In drug development processes, effective chemicals targeting especially the treatment

Electronic supplementary material The online version of this article (https://doi.org/10.1007/s00775-019-01653-6) contains supplementary material, which is available to authorized users.

Extended author information available on the last page of the article

of common diseases are widely tested. Thiosemicarbazide-based structures with or without a metal are potentially useful molecules for symptoms that are arising from bacteria, viruses, and irregular cell mechanisms [1–4]. For this class of compounds, the clinical trials of a thiosemicarbazide derivative, 3-aminopyridine-2-carboxaldehyde-thiosemicarbazone (triapine), for treatment of some cancers should be noted as a significant advance [5, 6].

As opposed to the limited efficacy and undesirable side effects of current treatments for advanced cancers, some metal complexes have been reported to possess several favorable properties suited to the anticancer drug design. From this point of view, the development of metallic complex drugs which can be activated in a controlled manner towards specific targets, with well-characterized speciation behavior, is of paramount importance [7, 8]. The study of binding metal complexes to DNA has a remarkable importance for the development of effective chemotherapy metal-based drugs, because the primary target is DNA for many antitumor drugs [9].

There are many publications concerning the biological properties of metal complexes with NS, ONS, and ONN-chelating thiosemicarbazones derived using various carbonyl compounds [10–13]. Because palladium, platinum or copper ions somehow guarantee a biological activity, these ions have been frequently preferred to obtain the thiosemicarbazone complexes [14, 15]. In 2007, some iron(III) complexes of tetradentate thiosemicarbazones having a selective cytotoxic effect on K562 leukemia cells were announced as an output of our research [16]. These thiosemicarbazone complexes are similar to the metallo-salen compounds in terms of *O*,*N*,*N*,*O*-chelating set and they are the biologically active structures. We also reported the antioxidant properties of some iron(III), nickel(II) and oxovanadium(IV) complexes having these N_2O_2-thiosemicarbazidato ligands in addition to cytotoxicity [16–20].

At this stage, the manganese ion that is functional in many enzyme systems and iron ion that proves an additional contribution for cytotoxicity in such complexes were investigated as metal centers (Fig. 1). Synthesis, structural analysis, cytotoxicity, and DNA interaction of the title complexes are the main topics of the paper. The manganese was employed for the first time in such N_2O_2 chelate complexes obtained from acetylacetone-*S*-methyl-thiosemicarbazone and in particular, it was aimed to compare the biological activity potential of manganese and iron ions in the thiosemicarbazide-based molecule designs.

Materials and methods

Analytical data were obtained with a Thermo Finnigan Flash EA 1112 analyzer. Infrared spectra were obtained using ATR unit in 4000–600 cm^{-1} range on Agilent Carry 630 spectrophotometer. UV–visible spectra were recorded on Ocean Optics QE65000 diode array spectrophotometer. ^1H and ^{13}C NMR spectra (in DMSO-d_6) were obtained using Varian UNITY INOVA 500 MHz NMR spectrometer. The molar conductivities of the complexes were measured in 10^{-3} M DMSO solution on a digital CMD 750 conductivity meter. Magnetic moment measurements were carried out by the Gouy technique with an MK I model device of Sherwood Scientific at room temperature.

Synthesis

The starting material, acetylacetone-S-methyl-thiosemicarbazone hydrogen iodide, was synthesized according to the reported procedures [21, 22]. The structure of cream-colored solid compound was checked by means of elemental analysis, infrared (ATR, cm^{-1}) and ^1H NMR (ppm, in dmso-d_6) spectra. *Anal. Calc*. for $C_7H_{14}N_3OSI$ (315.17): C, 26.68; H, 4.48; N, 13.33; S, 10.17. Found: C, 26.51; H, 4.23; N, 13.07; S, 9.91%. IR: $\nu_{as}(NH_2)$ 3327, $\nu_s(NH_2)$ 3260, ν(OH) 3184, $\delta(NH_2)$, $\nu(C{=}N^1)$, $\nu(N^2{=}C)$ 1637–1539. ^1H NMR: 9.39, 8.95 (*cis*/*trans* ratio:1/3, s, 2H, NH_2), 7.70 (s, 1H, OH), 3.23 (s, 2H, $–CH_2–$), 2.59 (s, 3H, S-CH_3), 2.08 (s, 3H, C–CH_3), 1.73 (s, 3H, C–CH_3). ^{13}C NMR: 165.31 (*4*), 164.75 (*6*), 96.21 (*2*), 58.44 (*3*), 26.07 (*1*), 16.69 (*7*), 13.92 (*5*).

For the synthesis of iron(III) complex (Fe1), to the solution of $FeCl_3$. $6H_2O$ (0.27 g, 1 mmol) in 5 mL of ethanol, a ligand solution was added (0.32 g, 1 mmol acetylacetone-*S*-methyl-thiosemicarbazone hydrogen iodide and 0.14 g, 1 mmol 4-hydroxy-salicylaldehyde were dissolved in 5 mL of ethanol). The mixture was stirred at 50 °C for 15 min and triethylamine (0.1 mL) was added to the solution. After several days, the dark red precipitate was filtered and recrystallized from a mixture of ethanol–dichloromethane (1:1, v/v). The yield is 0.12 g (30%).

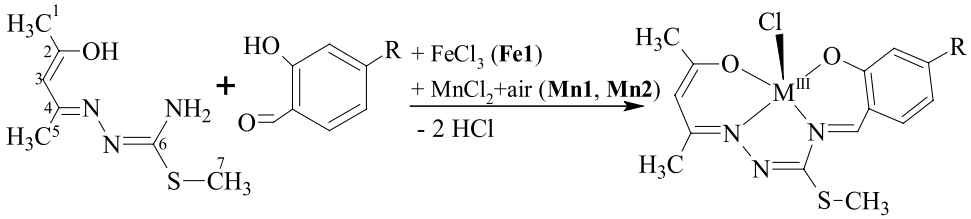

Fig. 1 Synthesis scheme of the complexes. M, R: Fe, OH (Fe1); Mn, H (Mn1); Mn, OCH_3 (Mn2)

The synthesis of Mn1 and Mn2 was performed as seen above using $MnCl_2.4H_2O$ and the aldehydes shown in Fig. 1. But there was a slight difference, air was bubbled through the mixture for 1 h at the end of the reaction time. After recrystallization, the manganese complexes were gained with relatively low yields, 0.095 g (25% for Mn1) and 0.082 g (20% for Mn2).

The μ_{eff} value (BM), molar conductivity (Ω^{-1} cm^2 mol^{-1}), elemental analysis, UV–Vis [in 10^{-5} M $CHCl_3$, λ_{max} (nm), log ε (dm^3 cm^{-1} mol^{-1})], and infrared (ATR, cm^{-1}) data of the complexes are:

Fe1: *Monochloro N^1-pentane-2,4-dione-N^4-2,4-dihydroxybenzylidene-S-methyl-thiosemicarbazidato-iron(III).* m.p: > 350 °C, 5.84, 14.4, *Anal. Calc.* for $C_{14}H_{15}N_3O_3SFeCl$ (396.65 g/mol): C, 42.39; H, 3.81; N, 10.59; S, 8.08. Found: C, 42.15; H, 3.65; N, 10.43; S, 7.85%. UV–Vis: 240 (4.86), 298 (5.04), 352 (4.84), 428 (4.71), 465 (4.48), 489 (4.28). IR: ν(O–H) 3329, ν(C=N^1) 1612, ν(N^2=C) 1594, ν(N^4=C) 1581, ν(C–O) 1150, 1126.

Mn1: *Monochloro N^1-pentane-2,4-dione-N^4-2-hydroxybenzylidene-S-methyl-thiosemicarbazidato-manganese(III).* m.p: > 350 °C, 4.86, 12.8, *Anal. Calc.* for $C_{14}H_{15}N_3O_2SMnCl$ (379.75 g/mol): C, 44.28; H, 3.98; N, 11.07; S, 8.44. Found: C, 43.97; H, 3.71; N, 10.81; S, 8.19%. UV–Vis: 243 (5.07), 285 (4.91), 372 (4.57), 412 (4.56), 435 (4.59), 493 (4.27), 575 (3.90). IR: ν(C=N^1) 1605, ν(N^2=C) 1572, ν(N^4=C) 1560, ν(C–O) 1140, 1120.

Mn2: *Monochloro N^1-pentane-2,4-dione-N^4-2-hydroxy-4-methoxybenzylidene-S-methyl-thiosemicarbazidato-manganese(III).* m.p: > 350 °C, 4.82, 16.2, *Anal. Calc.* for $C_{15}H_{17}N_3O_3SMnCl$ (409.77 g/mol): C, 43.97; H, 4.18; N, 10.25; S, 7.83. Found: C, 43.75; H, 4.04; N, 10.01; S, 7.35%. UV–Vis: 239 (4.92), 279 (5.06), 369 (4.11), 421 (3.88), 439 (3.79), 473 (3.69). IR: ν(C=N^1) 1611, ν(N^2=C) 1598, ν(N^4=C) 1577, ν(C–O) 1144, 1118.

X-ray diffraction analysis

Suitable crystals of Fe1 and Mn1 were selected for data collection which was performed on a Bruker D8-QUEST diffractometer equipped with a graphite–monochromatic Mo–K_α radiation at 296 K. The structures were solved by direct methods using SHELXS-2013 [23] and refined by full-matrix least-squares methods on F^2 using SHELXL-2013 [24]. All non-hydrogen atoms were refined with anisotropic parameters. The H atoms were located from different maps and then treated as riding atoms with C–H distance of 0.93–0.96 Å and O–H distance of 0.82 Å. The following procedures were implemented in our analysis: data collection, Bruker APEX2 [25]; the program used for molecular graphics, MERCURY programs [26]; the software used to prepare material for publication, WinGX [27]. Details of data collection and crystal structure determination are given in Table 1.

DNA-binding studies

Absorption spectrophotometric studies

The stock solution of DNA was prepared by dissolving of DNA in 5 mM Tris–HCl/50 mM NaCl buffer pH 7.2. The UV absorbance at 260 and 280 nm of the solution of CT-DNA in Tris–HCl/NaCl buffer pH 7.2 gives a ratio of 1.8–1.9, indicating that the DNA was sufficiently free of protein [28]. The DNA concentrations were detected from its absorption intensity at 260 nm with a molar extinction coefficient of 6600 M^{-1} cm^{-1} [29]. The absorption spectra of complexes binding to CT-DNA were performed by increasing the amount of CT-DNA added to the complexes in Tris–HCl/NaCl buffer pH 7.2 [30]. To compare the DNA-binding affinities of these complexes quantitatively, the absorbance was recorded after each addition of CT-DNA. The binding constants K_b of the complexes to CT-DNA were obtained using the following Wolfe–Shimer equation (Eq. 1) [31–33]:

$$[\mathrm{DNA}]/(\varepsilon a-\varepsilon f) = [\mathrm{DNA}]/(\varepsilon b-\varepsilon f) + 1/K_b(\varepsilon b-\varepsilon f) \quad (1)$$

Table 1 Crystal data and structure refinement parameters for Fe1 and Mn1

	Fe1	Mn1
Empirical formula	$C_{14}H_{15}ClFeN_3O_3S$	$C_{14}H_{15}ClMnN_3O_2S$
Formula weight	396.65	379.74
Crystal system	Triclinic	Triclinic
Space group	P-1	P-1
a (Å)	7.6509 (14)	7.7664 (8)
b (Å)	9.403 (2)	9.2578 (9)
c (Å)	12.964 (3)	12.3895 (14)
α (°)	76.701 (9)	76.919 (5)
β (°)	73.874 (8)	75.151 (5)
γ (°)	70.601 (9)	69.289 (4)
V (Å^3)	835.3 (3)	796.29 (15)
Z	2	2
D_c (g cm^{-3})	1.577	1.584
μ (mm^{-1})	1.20	1.14
θ range (°)	2.9–26.5	3.0–27.1
Measured reflections	19399	18465
Independent reflections	3361	2886
R_{int}	0.053	0.051
S	1.10	1.19
R1/wR2	0.088/0.214	0.099/0.251
$\Delta\rho_{max}/\Delta\rho_{min}$ (eÅ^{-3})	1.10/− 0.56	1.25/− 0.62

where εa, εf, and εb, are the apparent, free and bound metal complex extinction coefficients, respectively. In particular, εa was determined as the ratio between the measured absorbance and the samples' concentrations; A/[complex (M)], εf was determined by a calibration curve of the isolated metal complex in aqueous solution. Plot of [DNA]/($\varepsilon b - \varepsilon f$) versus [DNA] gave a slope of $+1/(\varepsilon b - \varepsilon f)$ and a Y intercept equal to $1/K_b(\varepsilon b - \varepsilon f)$ [34–37].

$$H\% = \left[\left(A_{\text{Free}} - A_{\text{Bound}}\right)/A_{\text{Free}}\right] \times 100\% \quad (2)$$

In this equation (Eq. 2), A_{Free} represents the absorbance intensity of the complex in the free state, while A_{Bound} represents the absorbance intensity of the complex after the DNA is added at the maximum concentration.

DNA cleavage

pBR322 plasmid DNA was used for all cleavage activities. In the experiment, 3 µL of plasmid DNA (0.5 µg/µl) was mixed with the different concentrations of complexes solved in 1% DMSO, respectively. Finally, the reaction mixture was diluted with the 10 mM Tris–HCl/50 mM NaCl buffer pH 7.22 to a total volume (30 µL). After that, the reaction mixtures were incubated at 37 °C for 1 h. Samples (15 µL) were then incubated at 37 °C and loaded with 4 µL of loading dye (10 mM Tris–HCl pH 7.6, 0.03% bromophenol blue, 0.03% xylene cyanol FF, 60% glycerol 60 mM EDTA), on 1% agarose gel. The gel was run at 70 V for 45 min in TAE buffer. After electrophoresis, the gel was stained with an ethidium bromide solution for 15 min. The gel was then destained for 10 min by keeping it in sterile distilled water and photographed in UV light [38, 39].The extent of cleavage of the SC DNA was determined by measuring the intensities of the bands using the Gel Documentation System (BIO-RAD, İmage Lab™ Software Version 5.2.1) [40, 41].

Cell cultures

Human cervical carcinoma (HeLa, ATCC® CCL-2™) and human colorectal adenocarcinoma (HT-29, ATCC® HTB-38™) cell lines were grown in Dulbecco's modified Eagle's medium (DMEM) (Life Tech) supplemented with 10% fetal bovine serum (Life Tech), 100 IU/mL penicillin, 100 mg/mL streptomycin (Life Tech.), and 2 mM L-glutamine (Life Tech). Cell culturing was carried out at 37 °C with 95% air and 5% CO_2. The cultures medium was renewed every alternate day. When these cells reached 80% confluence, the assay performed.

Cell viability assay

The 3-(4,5-dimethylthiazol-2-yl)-2,5-diphenyltetrazolium bromide (MTT) assay was used to evaluate the cell viability of complexes on HT-29 and HeLa cell lines according to the method of Mosmann with some modifications [42]. Prior to the treatment of the complexes, 1×10^4 cells/well (200 µl/well) were seeded into a 96-well tissue culture plate, then the different concentrations (0, 10, 25, 50, 100, 250, 500, and 1000 µM for Fe1; 0, 100, 250, 500, and 1000 µM for complexes Mn1 and Mn2) of the test samples dissolved in DMSO were added. As controls, cells were treated with DMEM (negative control) and DMEM with DMSO (positive control). For cell viability assays, HT-29 and HeLa cells were plated in 96-well plates at a density of 1×10^4 cells/well. After a 24 h incubation period at 37 °C, the culture medium was completely removed and 20 µL of 3-(4,5-dimethylthiazol-2-yl)-2,5-diphenyltetrazolium bromide (MTT—5 mg/mLin PBS) was added. After incubation at 37 °C for 4 h, the MTT solution was removed from each wells and the formazan crystals generated were solubilized using 200 µL of DMSO at 37 °C and the optical density of samples was measured using a microplate reader (Epoch, BioTek) at 570 nm to compute cell survival rate. All experiments were performed in triplicate and expressed as mean ± SD. The non-treated cells were deemed as control group. The cell viability was determined by comparing the absorbance of the treated cells with that of the control. The 50% inhibition concentration (IC_{50}) was defined as the complex concentration causing 50% inhibition of cell growth and was calculated using linear regression analysis [43, 44]. Cell viability % = (Mean absorbance in test wells/Mean absorbance in control wells) × 100.

Statistical analysis

For the cell viability analysis, four replicates were used in all experiments and values are expressed as means ± standard error. One Way ANOVA test was used to calculate the significance between the means, and Tukey test was used to compare averages. P values < 0.05 were considered to be statistically significant.

Results and discussion

Synthesis and spectroscopic data

The complexes, Fe1, Mn1, and Mn2, were gained by reaction of acetylacetone-*S*-methyl-thiosemicarbazone and the salicylaldehydes in presence of iron or manganese ion (Fig. 1). The aerial oxidation of manganese(II) to manganese(III) yielded the complexes in general formula [Mn^{III}(L)Cl]. The complexes, [M^{III}(L)Cl], having a dibasic thiosemicarbazidato ligand (L^{2-}) are in crystalline form, and soluble in alcohols and chlorinated hydrocarbons.

The template condensation and coordination of the thiosemicarbazidato ligand are simultaneous and the reaction could be monitored by comparing the infrared spectra of *S*-methyl-thiosemicarbazone and metal complex. *S*-methyl-thiosemicarbazone clearly exhibits the ν(OH), $\nu(NH_2)$, $\delta(NH_2)$, $\nu(C{=}N^1)$, and $\nu(N^2{=}C)$ bands. After reaction, the bands related to the OH and NH_2 groups were not recorded due to the connection of deprotonated form of thiosemicarbazidato (L^{2-}) backbone [45]. In ^{1}H-NMR spectra of the S-methyl-thiosemicarbazone, *cis–trans*-isomer peaks of N^4H_2 protons were observed at 9.39, 8.95 ppm. The OH proton on acetylacetone moiety was recorded at 7.70 ppm (Figure S3). The ^{13}C NMR spectra displayed the C(4), C(6), C(2) and C(3) signals expected for the thiosemicarbazone at 165.31, 164.75, 96.21 and 58.44 ppm, respectively (Figure S4).

Electronic spectra of the complexes contain the bands in the region of 239–243, 279–298, and 352–372 nm arising from $\pi \rightarrow \pi^*$ and $n \rightarrow \pi^*$ transitions belonging to azomethine and thioamide groups. In 412–575 nm zone of the complex spectra were observed the LMCT bands [46, 47]. The electronic spectra of the complexes did not give any finding belonging to the square pyramidal structures explicated by X-ray analysis, probably because of low intensities of *d–d* transitions.

The molar conductances of the complexes are between 12.8 and 16.2 Ω^{-1} cm^2 mol^{-1} considerably lower than the limit value accepted as 80 and indicate the non-ionic structures. The complexes have the paramagnetic metal ions with a high-spin state. The obtained μ_{eff} value of Fe1 (5.84 BM) indicates the five unpaired d^5 structure. The BM values of Mn1 (4.86) and Mn2 (4.82) are equivalent to four unpaired electrons in the d^4 structure.

Crystal structures

The molecular structures of complexes Fe1 and Mn1, with the atom numbering schemes, are shown in Figs. 2 and 3, and details of data collection and crystal structure determinations are given in Table 1.

The asymmetric units of complexes Fe1 and Mn1 contain one thiosemicarbazidato ligand, one metal ion (Fe^{III} in Fe1 and Mn^{III} in Mn1), and one chlorine atom as displayed in Figs. 2 and 3. The coordination geometry around Fe^{III} and Mn^{III} ions can be described as a distorted square pyramidal geometry. Using Addison tau parameter (τ) enables the distinction between trigonal bipyramidal (ideally $\tau = 1$) and square pyramidal (ideally $\tau = 0$) geometries [48, 49]. Considering the angles O1–Fe1–N3 (150.9°) and O3–Fe1–N1 (144.6°) for Fe1, O1–Mn1–N3 (159.6°) and O2–Mn1–N1 (156.9°) for Mn1 (Table 2), the τ values are calculated. The values of τ for the Fe^{III} and Mn^{III} ions are 0.105 and 0.045, respectively, indicating slightly distorted square pyramids.

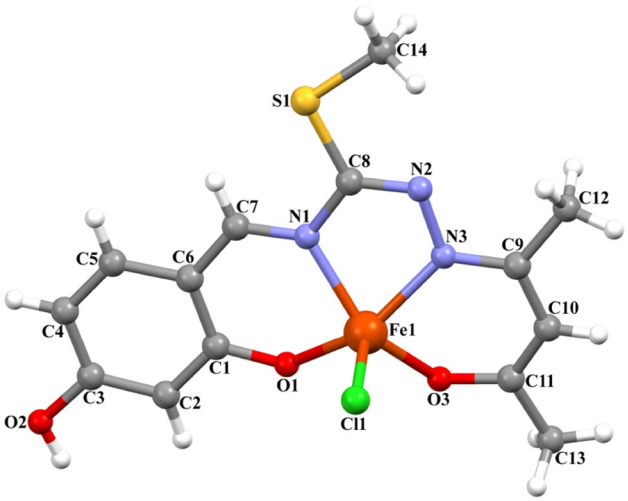

Fig. 2 The molecular structures of complex Fe1 showing the atom numbering schemes

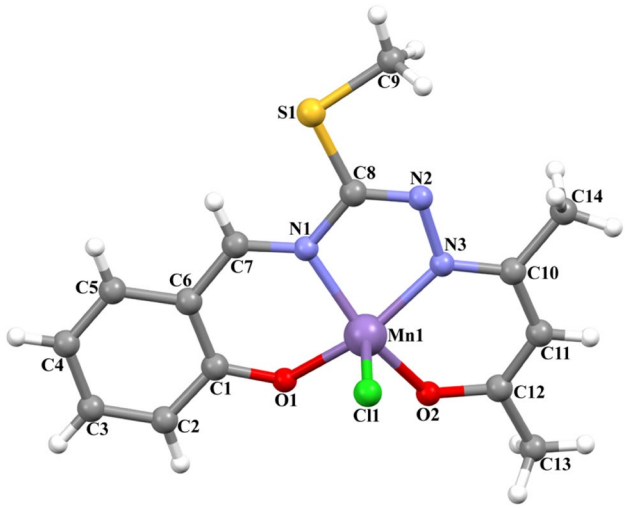

Fig. 3 The molecular structures of complex Mn1 showing the atom numbering schemes

In both complex structures, the metal ions are coordinated with two oxygen atoms [Fe1–O1 = 1.907(5) Å and Fe1–O3 = 1.897(6) Å for Fe1 and Mn1–O1 = 1.867(6) Å and Mn1–O2 = 1.882(6) Å for Mn1] and two nitrogen atoms [Fe1–N1 = 2.061(6) Å and Fe1–N3 = 2.047(6) Å for Fe1 and Mn1–N1 = 1.995(7) Å and Mn1–N3 = 1.952(7) Å for Mn1]. The chlorine atoms at the top of the square pyramid structures are relatively weak bonded. The bond lengths are 2.268(2) Å of Fe1–Cl and 2.440(2) Å of Mn1–Cl.

In crystal of Fe1, atom O2 in the molecule at (x, y, z) acts as hydrogen bond donor to the Cl1 atom in the molecule at ($1 - x$, $2 - y$, $1 - z$), so forming a centrosymmetric $R_2^2(16)$ ring centered at (1/2, 1, 1/2). In complex Mn1, the weak

Table 2 Selected bond distances and angles (Å, °)

Fe1					
Fe1–Cl1	2.268 (2)	Fe1–O3	1.897 (6)	Fe1–O1	1.907 (5)
Fe1–N3	2.047 (6)	Fe1–N1	2.061 (6)		
O3–Fe1–O1	93.8 (3)	O3–Fe1–N3	87.8 (3)	O1–Fe1–N3	150.9 (3)
O3–Fe1–N1	144.6 (3)	O1–Fe1–N1	87.3 (2)	N3–Fe1–N1	75.2 (3)
O3–Fe1–Cl1	106.4 (2)	N3–Fe1–Cl1	101.8 (2)	N1–Fe1–Cl1	107.34 (19)
Mn1					
Mn1–Cl1	2.440 (2)	Mn1–O1	1.867 (6)	Mn1–O2	1.882 (6)
Mn1–N3	1.952 (7)	Mn1–N1	1.995 (7)		
O1–Mn1–O2	91.1 (3)	O1–Mn1–N3	159.6 (3)	O2–Mn1–N3	91.2 (3)
O1–Mn1–N1	90.5 (3)	O2–Mn1–N1	156.9 (3)	N3–Mn1–N1	79.7 (3)
O2–Mn1–Cl1	103.4 (3)	N3–Mn1–Cl1	98.2 (2)	N1–Mn1–Cl1	98.9 (2)

intermolecular $\pi\ldots\pi$ interactions play a major role in constructing network.

DNA-binding study

Gene expression errors can cause diseases; therefore, understanding DNA–drug binding is essential for the rationale design of anticancer drugs [50–53]. Electronic absorption spectroscopy is the most widely used method for detecting the interaction of small molecules with DNA and formation of their complex [54]. When a small molecule interacts with DNA, changes in the absorbance and/or in the position of peak are observed [55]. Hyperchromic and hypochromic effects are the spectral properties of DNA regarding its double-helical structure [56, 57]. Hypochromism is caused by the contraction of DNA in the helix axis, as well as by the conformational change on DNA; on the contrary, hyperchromism originates from the damage to the DNA double helix structure [57–59]. The strength of interaction is correlated with the magnitude of shifting in the peak position or changes in absorbance [60, 61]. In general, hypochromism and a red shift (bathochromism) of the absorption band means intercalative mode of binding owing to strong stacking interaction between the base pairs of the DNA, and the planar aromatic chromophore (1,10-phenanthroline) [62], while hyperchromism is a spectral property showing non-covalent interactions, especially electrostatic, groove binding, etc. resulting from the damage of DNA double helix structure.

Transition metal complexes can bind to DNA through both covalent and/or non-covalent interactions [35]. As shown in Fig. 4, the absorption intensity of the complex Fe1 increased (hyperchromism) with a decrease in the absorption wavelength (red shift). On the other hand, the absorption intensity of complexes Mn1 and Mn2 increased (hyperchromism) with a rise in the absorption wavelength (blue shift) upon addition of CT-DNA.

The bands of complex Fe1 at 278.8 nm exposes a hyperchromism and a red shift (bathochromism) of 33.2 nm (up to 245.6 nm), suggesting the combined covalent and non-covalent intercalative binding of Fe1 to DNA by the insertion of the planar moiety of the complex between adjacent base pairs on the DNA duplex. This is a typical hyperchromic effect which suggests that the DNA double helix structure is damaged after interaction with complex Fe1 through intercalation mode involving a strong stacking interaction between chromophore backbone of the ligand and the base pairs of DNA [57–59].

Similar findings are found in some studies. Lazic et al. showed that water-soluble ruthenium (II) terpyridine complexes cause hyperchromism and red shift. [63]. Milutinovic et al. also reported that a camphor based 1,3-diamine Ru(II) terpyridine complex causes hyperchromism and red shift [64]. These results suggest that the complexes are linked to CT-DNA by intercalation mode.

The manganese complexes showed hyperchromism with blue shifts of 7.6 nm (for Mn1) and 7.0 nm (for Mn2). The band of Mn1 shifted from 236.60 to 244.2 nm, and the band of Mn2 from 235.0 to 242.0 nm. In this case, a groove binding and/or electrostatic interactions can be suggested rather than the intercalative mode for interaction between the manganese complexes and CT-DNA. The findings are compatible with literature data. Sarwar et al. reported that esculetin complexes cause a hyperchromism attributing groove binding and/or electrostatic interactions rather than the intercalative mode of interaction between esculetin and CT-DNA [64].

To conduct a further research on the intensity of the interaction, the intrinsic binding constant (Kb) between the complexes (Fe1, Mn1 and Mn2) and CT-DNA were calculated. The Kb values which follows the order Fe1 > Mn2 > Mn1 clearly revealed the affinity of Fe1 to DNA is greater than that of manganese complexes (Table 3).

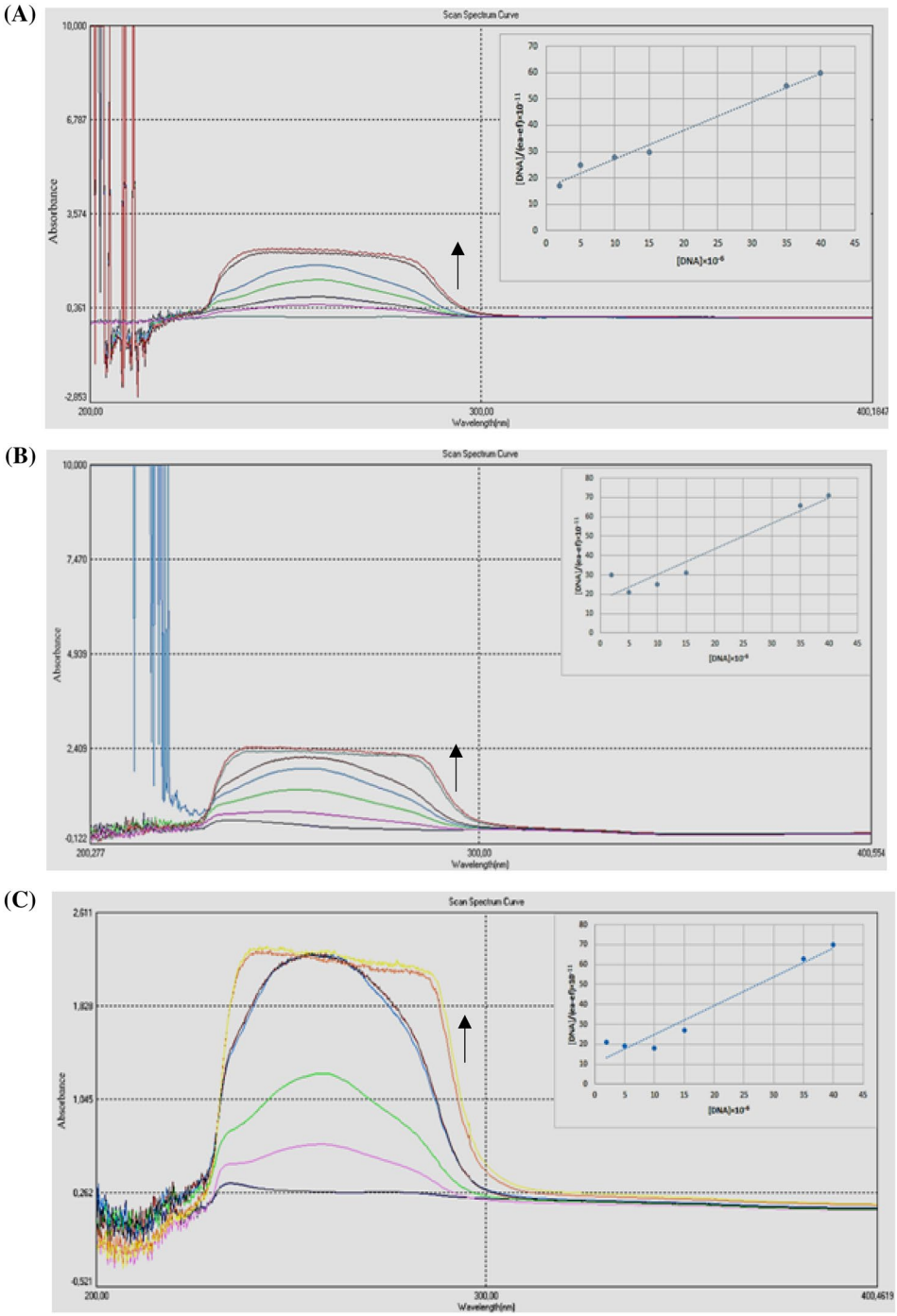

Fig. 4 Electronic absorption spectra of **a** complexes Fe1, **b** Mn1 and **c** Mn2 in the absence and in the presence of increasing amount of DNA concentrations. Arrow shows the absorbance changes upon increasing DNA concentrations. Plot of [DNA] vs [DNA]/$\varepsilon_a - \varepsilon_f$ for the titration of CT-DNA with the complexes. [Complex]: 35 µM. [DNA]: (2, 5, 10, 15, 35, 40) µM

DNA cleavage activity

Binding of transition metal complexes with DNA plays an important role in the recognition of chemotherapeutic candidates based on DNA cleavage [65]. It is believed that the anticancer activities of metal complexes are attributed to their abilities to bind DNA, to damage its structure and to disrupt its function [66]. The change in the electrophoretic mobility of plasmid DNA on gel usually indicates direct DNA–metal interaction [53]. When circular plasmid DNA is conducted by gel electrophoresis, the fastest migration will be observed for the supercoiled (SC) form of DNA (Form I). If one strand is cleaved, the supercoils will relax to produce a slower-moving nicked circular (NC) form of DNA (Form II). If both strands are cleaved, a linear form of DNA (Form III) will be generated that migrates in between [30, 62, 67, 68].

In the study, the DNA–metal complex interaction as DNA cleavage was performed with supercoiled (SC)

Table 3 Interaction and spectral parameters of the complexes with calf thymus DNA

Complexes	λ_{max} (nm)		$\Delta\lambda$ (nm)	H %[a]	K_b (M^{-1})[b]
	Free	Bound			
Fe1	278.80	245.60	33.2 (red shift)	39.73	1×10^5
Mn1	236.60	244.20	7.6 (blue shift)	4.01	0.7×10^5
Mn2	235.00	242.00	7.0 (blue shift)	5.78	0.8×10^5

[a]$H\,\% = [(A_{free} - A_{bound})/A_{free}]\times100\%$, where H % is the percentage of hyperchromicity [37]

[b]K_b = Intrinsic DNA-binding constant determined from the UV–Vis absorption spectral titration

pBR322 DNA as a substrate using different concentrations of the complexes. No significant cleavage was found in the presence of complex Mn1 and Mn2. With increasing concentrations of complex Fe1, it was determined that Form I plasmid DNA gradually converted into Form II, which clearly implicates the role of metal ion in the process of DNA cleavage. It was clearly seen that complex Fe1 was found to promote the cleavage of DNA from supercoiled Form I (SC) to nicked circular Form II (NC) with simultaneous increase in the intensity of the latter form. Similarly, Tabassum et al. reported that as the concentration of a copper(II) Schiff-based complex was incremented, there was an important conversion of SC form to NC form which clearly indicates the role of metal ion in the process of DNA cleavage [69]. Especially at 2000 and 3000 µM concentrations of complex Fe1, a better cleavage activity was observed compared to other concentrations (Fig. 5). Thus, it was clear that the cleavage of pBR322 DNA was directly correlated with higher DNA-binding ability of complex Fe1.

Similarly, Deng et al. reported that this can be predicated by the fact that interactions of the Ni(II) complexes with pBR322 DNA can relax the supercoiled form, thus the plasmid DNA cleavage ability was related to the DNA-binding ability of the Ni(II) complexes [70]. Also, it was reported that the DNA cleavage efficiencies were related to the DNA-binding affinity of water-soluble copper(II)–dipeptide complexes [71] and Cu(II) complex of L-enantiomeric fluoro-substituted benzothiazole Schiff-based valine [72]. In addition, Kumari et al. indicated that cleavage was directly connected with high DNA-binding propensities of tri- and diorganotin(IV) derivatives of non-steroidal anti-inflammatory drug sulindac [73]. Annaraj et al. reported that the amount of helical unwinding induced by the complex bound to SC DNA provides evidence for the intercalation mode of interaction between the ligand copper(II) complexes containing a phenylalanine derivative and diimine co-ligands and DNA [74].

Our results indicated that, the amount of helical unwinding induced by the complex Fe1 bound to SC DNA provides evidence for the intercalation mode of interaction between the Fe1 and DNA. The relationship between DNA-binding ability and cleavage activity with pBR322 DNA of Fe1 was determined, and the ability of Fe1 to serve as a metallonuclease was studied with pBR322 DNA cleavage at different concentrations.

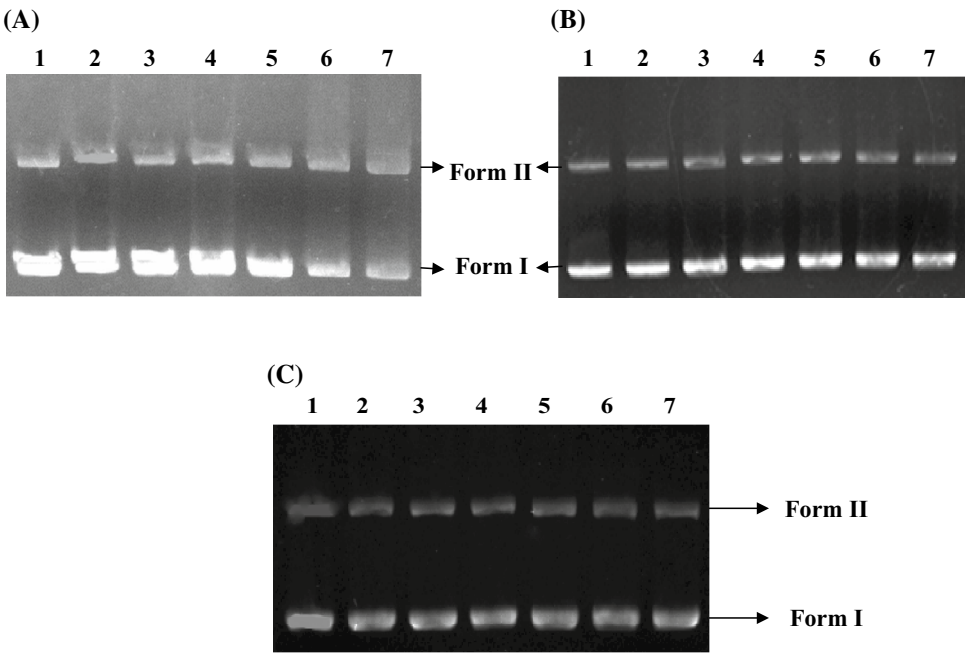

Fig. 5 Gel electrophoresis diagram showing the cleavage to pBR322 DNA (0.5 µg/µl) in the presence of varying concentrations of the complexes. Line 1, DNA control; Line 2–7, pBR322 DNA in the presence of Fe1 (**a**) (50, 100, 200, 500, 2000, 3000 µM), Mn1 (**b**) (50, 100, 200, 500, 1000, 4000 µM) and Mn2 (**c**) (50, 100, 200, 1000, 2000, 3000 µM)]

Anti-proliferative effect of complexes on HT-29 and HeLa

The inhibitory effect of different concentrations of complexes on HT-29 and HeLa cell lines was assessed by MTT assay following 24 h of treatment. The anti-proliferative effect of complexes on HT-29 cells was concentration dependent at 24 h time points (Figs. S1, S2). The complex Fe1 exhibited more anti-proliferative effect on HT-29 and HeLa cells at all concentrations than complexes Mn1 and Mn2. The highest anti-proliferative effect on HT-29 and HeLa cells was observed in the application of Fe1 at 100–1000 µM (92%) and 50–250 µM (92–93%) concentrations, respectively. Only 1000 µM of Mn2 showed a high anti-proliferative effect on HT-29 (62%) and HeLa (68%) cells. In addition, IC_{50} values of complexes, whose concentration causing 50% inhibition of cell proliferation, were determined as µM and the related results are shown in Table 4. The greatest growth inhibitory activity against HT-29 and HeLa cell lines was exhibited by Fe1 with IC_{50} at 16 µM and 11 µM, respectively.

In anti-proliferation experiments of the complexes on HT-29 and HeLa cell lines, Fe1 showed better cytotoxic activity depending on the increase of concentration compared to other complexes. The order of anti-proliferation activity is Fe1 > Mn2 > Mn1. According to the study by Manan et al., the anti-proliferative activities of centrosymmetric copper(II) complex derived from S-methyldithiocarbazate with isatin were categorized into four groups: $IC_{50} < 5.0$ µg/mL = strongly active, $IC_{50} = 5.0–10.0$ µg/mL = moderately active, $IC_{50} = 10–25.0$ µg/mL = weakly active, $IC_{50} > 25.0$ µg/mL = inactive [75]. Accordingly, only Fe1 showed strong anti-proliferative activity at HT-29 and HeLa cell lines. According to the US National Cancer Institute (NCI) anticancer compound screening program, a plant extract is generally considered to have an active cytotoxic effect if the IC_{50} value following incubation between 48 and 72 h is 20 µg/mL or less [76, 77]. The compounds having IC_{50} values ≤ 20 µg/mL against any human cell line can be classified as highly cytotoxic (or anti-proliferative). In this study, compared with the scale given above, it is observed that the application of Fe1, for 24 h has a high cytotoxic effect on the HeLa and HT-29 cell lines.

As a result, it has been found that the antitumor activity of complexes was related to both DNA-binding and DNA cleavage activity. Similarly, Fu et al. reported that the in vitro cytotoxicity toward HepG2, HeLa, A549 and U87 cell lines for two water-soluble copper(II)–dipeptide complexes: $[Cu(glygly)(PyTA)]ClO_4 \cdot 1.5H_2O$ (1) and $[Cu(glygly)(PzTA)]ClO_4 \cdot 1.5H_2O$ (2) follows the order 1 > 2, which coincides with the DNA cleavage activities of the two complexes [71]. This fact indicates that the antitumor activity for the complexes may be closely related to their DNA interaction.

Table 4 The anti-proliferative activity in vitro expressed as IC_{50} (µM) values of the complexes against HT-29 and HeLa cell lines after 24 h incubation time

Cell lines	IC_{50} (µM)		
	Fe1	Mn1	Mn2
HT-29	16	1059	903
HeLa	11	2963	822

The IC_{50} value was determined as that concentration causing 50%

Inhibition of cell proliferation ($T/C_{corr} = 50\%$)(µM) [43, 44]

Conclusions

The synthesis and structural analysis of the new thiosemicarbazone-based complexes containing iron and manganese in the 3 + oxidation step were performed. The activity comparison depending on the metal ions and aromatic substituents was revealed using the methods as mentioned above.

The significant results serving the purpose of the bioactive molecules which can be useful in cancer control were obtained. All complexes showed anti-proliferative effects, but Fe1 especially has higher anticancer activity even at low concentrations than the manganese complexes. In the experiments indicating that iron metal is more effective, the anti-proliferation enhancing the influence of hydroxy and methoxy groups was clearly observed. The complex Fe1 with the hydroxy substituent and iron(III) center exhibited a clear superiority against the manganese complexes, Mn1 and Mn2. The contribution of the methoxy group on activity was seen also in the manganese complexes by resulting in Mn2 being more effective than Mn1. DNA-binding ability and cleavage activity of complex Fe1 is greater than the others. Considering the order in efficiency (Fe1 > Mn2 > Mn1) in anti-proliferation and DNA interaction, it can be said that manganese(III) center was not able to compete with iron(III) in this molecule design although Mn2 had a noteworthy activity.

By these findings, the anti-proliferative potency of Fe1 on HT-29 and HeLa cells is directly proportional with its DNA affinity. Eventually, the anticancer effect of Fe1 appears to be related to DNA-binding and DNA cleavage ability that has drawn a great deal of attention. Therefore, the iron (III) complex may be recommendable as a potential DNA-targeting anticancer agent. However, further research is required to elucidate the mechanism of action of iron(III) complex on its anticancer functionality.

Acknowledgements This work was supported by the Scientific Research Projects Coordination Unit of Istanbul University-Cerrahpasa. The authors acknowledge Scientific and Technological Research

Application and Research Center, Sinop University, Turkey, for the use of the Bruker D8-QUEST diffractometer.

References

1. Pahontu E, Julea F, Rosu T, Purcarea V, Chumakov Y, Petrenco P, Gulea A (2015) Antibacterial, antifungal and in vitro antileukaemia activity of metal complexes with thiosemicarbazones. J Cell Mol Med 19:865–878
2. Pelosi G, Bisceglie F, Bignami F, Ronzi P, Schiavone P, Re MC, Casoli C, Pilotti E (2010) Antiretroviral activity of thiosemicarbazone metal complexes. J Med Chem 53:8765–8769
3. da Silva JBP, do AF Navarro DM, da Silva AG, Santos GK, Dutra KA, Moreira DR, Ramos MN, Espíndola JWP, de Oliveira ADT, Brondani DJ (2015) Thiosemicarbazones as Aedes aegypti larvicidal. Eur J Med Chem 100:162–175
4. Dilworth JR, Hueting R (2012) Metal complexes of thiosemicarbazones for imaging and therapy. Inorg Chim Acta 389:3–15
5. Kunos CA, Chu E, Beumer JH, Sznol M, Ivy SP (2017) Phase I trial of daily triapine in combination with cisplatin chemotherapy for advanced-stage malignancies. Cancer Chemother Pharmacol 79:201–207
6. Mortazavi A, Ling Y, Martin LK, Wei L, Phelps MA, Liu Z, Harper EJ, Ivy SP, Wu X, Zhou B-S (2013) A phase I study of prolonged infusion of triapine in combination with fixed dose rate gemcitabine in patients with advanced solid tumors. Invest New Drugs 31:685–695
7. Ott I, Gust R (2007) Non platinum metal complexes as anti-cancer drugs. Arch Pharm 340:117–126
8. Patil SA, Patil SA, Patil R, Keri RS, Budagumpi S, Balakrishna GR, Tacke M (2015) N-heterocyclic carbene metal complexes as bio-organometallic antimicrobial and anticancer drugs. Future Med Chem 7:1305–1333
9. Sangeetha S, Murali M (2018) Non-covalent DNA binding, protein interaction, DNA cleavage and cytotoxicity of [Cu(quamol) Cl].H2O. Int J Biol Macromol 107:2501–2511
10. Khan T, Dixit S, Ahmad R, Raza S, Azad I, Joshi S, Khan AR (2017) Molecular docking, PASS analysis, bioactivity score prediction, synthesis, characterization and biological activity evaluation of a functionalized 2-butanone thiosemicarbazone ligand and its complexes. J Chem Biol 10:91–104
11. Balachandran C, Haribabu J, Jeyalakshmi K, Bhuvanesh NS, Karvembu R, Emi N, Awale S (2018) Nickel (II) bis (isatin thiosemicarbazone) complexes induced apoptosis through mitochondrial signaling pathway and G0/G1 cell cycle arrest in IM-9 cells. J Inorg Biochem 182:208–221
12. Zhang H, Thomas R, Oupicky D, Peng F (2008) Synthesis and characterization of new copper thiosemicarbazone complexes with an ONNS quadridentate system: cell growth inhibition, S-phase cell cycle arrest and proapoptotic activities on cisplatin-resistant neuroblastoma cells. J Biol Inorg Chem 13:47–55
13. Rettondin AR, Carneiro ZA, Gonçalves AC, Ferreira VF, Oliveira CG, Lima AN, Oliveira RJ, de Albuquerque S, Deflon VM, Maia PI (2016) Gold (III) complexes with ONS-Tridentate thiosemicarbazones: toward selective trypanocidal drugs. Eur J Med Chem 120:217–226
14. Matesanz AI, Jimenez-Faraco E, Ruiz MC, Balsa LM, Navarro-Ranninger C, León IE, Quiroga AG (2018) Mononuclear Pd (ii) and Pt (ii) complexes with an α-N-heterocyclic thiosemicarbazone: cytotoxicity, solution behaviour and interaction versus proven models from biological media. Inorganic Chem Front 5:73–83
15. Park KC, Fouani L, Jansson PJ, Wooi D, Sahni S, Lane DJ, Palanimuthu D, Lok HC, Kovačević Z, Huang ML (2016) Copper and conquer: copper complexes of di-2-pyridylketone thiosemicarbazones as novel anti-cancer therapeutics. Metallomics 8:874–886
16. Bal T, Atasever B, Solakoğlu Z, Erdem-Kuruca S, Ülküseven B (2007) Synthesis, characterisation and cytotoxic properties of the *N*1, *N*4-diarylidene-*S*-methyl-thiosemicarbazone chelates with Fe(III) and Ni (II). Eur J Med Chem 42:161–167
17. Atasever B, Ülküseven B, Bal-Demirci T, Erdem-Kuruca S, Solakoğlu Z (2010) Cytotoxic activities of new iron (III) and nickel (II) chelates of some *S*-methyl-thiosemicarbazones on K562 and ECV304 cells. Invest New Drugs 28:421–432
18. Kaya B, Atasever-Arslan B, Kalkan Z, Gur H, Ulkuseven B (2016) Apoptotic mechanisms of nickel (II) complex with *N*1-acetylacetone-*N*4-4-methoxy-salicylidene-*S*-allyl-thiosemicarbazone on HL60 leukemia cells. Gen Physiol Biophys 35:451–458
19. Bal-Demirci T, Şahin M, Özyürek M, Kondakçı E, Ülküseven B (2014) Synthesis, antioxidant activities of the nickel (II), iron (III) and oxovanadium (IV) complexes with N2O2 chelating thiosemicarbazones. Spectrochim Acta Part A Mol Biomol Spectrosc 126:317–323
20. Kaya B, Şahin O, Bener M, Ülküseven B (2018) Iron (III) and nickel (II) complexes with *S*-alkyl (*n*-C1-6)-thiosemicarbazidato ligands: synthesis, structural characterization, and antioxidant features. J Mol Struct 1167:16–22
21. Yamazaki C (1975) The structure of isothiosemicarbazones. Can J Chem 53:610–615
22. Gradinaru J, Forni A, Simonov Y, Popovici M, Zecchin S, Gdaniec M, Fenton DE (2004) Mononuclear nickel (II) and copper (II) complexes with Schiff base ligands derived from 2, 6-diformyl-4-methylphenol and S-methylisothiosemicarbazones. Inorg Chim Acta 357:2728–2736
23. Sheldrick GM (2008) A short history of SHELX. Acta Crystallogr A 64:112–122
24. Sheldrick GM (2015) SHELXT–Integrated space-group and crystal-structure determination. Acta Crystallogr Sect A Found Adv 71:3–8
25. Bruker S-N (2013) Data reduction software. Bruker AXS Inc, Madison, Wisconsin, USA
26. Macrae CF, Bruno IJ, Chisholm JA, Edgington PR, McCabe P, Pidcock E, Rodriguez-Monge L, Taylor R, Jvd Streek, Wood PA (2008) Mercury CSD 2.0–new features for the visualization and investigation of crystal structures. J Appl Crystallogr 41:466–470
27. Farrugia LJ (2012) WinGX and ORTEP for windows: an update. J Appl Crystallogr 45:849–854
28. Marmur J (1961) A procedure for the isolation of deoxyribonucleic acid from micro-organisms. J Mol Biol 3:208-IN201
29. Gultneh Y, Khan AR, Blaise D, Chaudhry S, Ahvazi B, Marvey BB, Butcher RJ (1999) Syntheses and structures of and catalysis of hydrolysis by Zn(II) complexes of chelating pyridyl donor ligands. J Inorg Biochem 75:7–18
30. Li DD, Tian JL, Gu W, Liu X, Zeng HH, Yan SP (2011) DNA binding, oxidative DNA cleavage, cytotoxicity, and apoptosis-inducing activity of copper(II) complexes with 1,4-tpbd (*N*, *N*, *N*', *N*'-tetrakis(2-yridylmethyl)benzene-1,4-diamine) ligand. J Inorg Biochem 105:894–901
31. Wolfe A, Shimer GH Jr, Meehan T (1987) Polycyclic aromatic hydrocarbons physically intercalate into duplex regions of denatured DNA. Biochemistry 26:6392–6396
32. Thompson KH, Orvig C (2006) Metal complexes in medicinal chemistry: new vistas and challenges in drug design. Dalton Trans 761–764
33. Pyle AM, Rehmann JP, Meshoyrer R, Kumar CV, Turro NJ, Barton JK (1989) Mixed-ligand complexes of ruthenium(II): factors governing binding to DNA. J Am Chem Soc 111:3051–3058
34. Jeyalakshmi K, Selvakumaran N, Bhuvanesh NSP, Sreekanth A, Karvembu R (2014) DNA/protein binding and cytotoxicity studies

of copper(ii) complexes containing *N*, *N*′, *N*″-trisubstituted guanidine ligands. RSC Adv 4:17179–17195
35. Borowska J, Sierant M, Sochacka E, Sanna D, Lodyga-Chruscinska E (2015) DNA binding and cleavage studies of copper(II) complexes with 2′-deoxyadenosine modified histidine moiety. JBIC 20:989–1004
36. Shahabadi N, Kashanian S, Darabi F (2009) In vitro study of DNA interaction with a water-soluble dinitrogen schiff base. DNA Cell Biol 28:589–596
37. Pravin N, Utthra PP, Kumaravel G, Raman N (2016) Effective DNA binding and cleaving tendencies of malonic acid coupled transition metal complexes. J Mol Struct 1123:162–170
38. Kulaksizoğlu S, Gökçe C, Güp R (2012) Synthesis and characterization of bis (azine) ligands and metal complexes: DNA-interaction and extraction properties for metals and dichromate anions. Turk J Chem 36:717–733
39. Netalkar PP, Netalkar SP, Budagumpi S, Revankar VK (2014) Synthesis, crystal structures and characterization of late first row transition metal complexes derived from benzothiazole core: anti-tuberculosis activity and special emphasis on DNA binding and cleavage property. Eur J Med Chem 79:47–56
40. Bernadou J, Pratviel G, Bennis F, Girardet M, Meunier B (1989) Potassium monopersulfate and a water-soluble manganese porphyrin complex,[Mn (TMPyP)](OAc) 5, as an efficient reagent for the oxidative cleavage of DNA. Biochemistry 28:7268–7275
41. Babu MS, Reddy KH, Krishna PG (2007) Synthesis, characterization, DNA interaction and cleavage activity of new mixed ligand copper (II) complexes with heterocyclic bases. Polyhedron 26:572–580
42. Mosmann T (1983) Rapid colorimetric assay for cellular growth and survival: application to proliferation and cytotoxicity assays. J Immunol Methods 65:55–63
43. Scheffler H, You Y, Ott I (2010) Comparative studies on the cytotoxicity, cellular and nuclear uptake of a series of chloro gold(I) phosphine complexes. Polyhedron 29:66–69
44. Rubner G, Bensdorf K, Wellner A, Bergemann S, Ott I, Gust R (2010) [Cyclopentadienyl]metal carbonyl complexes of acetylsalicylic acid as neo-anticancer agents. Eur J Med Chem 45:5157–5163
45. Ahmadi M, Mague JT, Akbari A, Takjoo R (2012) Dianion *N*1, *N*4-bis (salicylidene)-*S*-allyl-thiosemicarbazide complexes: synthesis, structure, spectroscopy and thermal behavior. Polyhedron 42:128–134
46. Kobayashi H, Yanagawa Y, Osada H, Minami S, Shimizu M (1973) Electronic spectra of high-spin iron (III) tetraphenylporphins. Bull Chem Soc Jpn 46:1471–1479
47. Habibi MH, Askari E (2013) Synthesis, structural characterization, thermal, and electrochemical investigations of a square pyramid manganese(III) complex with a Schiff base ligand acting as N_2O_2 tetradentate in equatorial and as O monodendate in axial positions: application as a precursor for preparation of Mn-doped ZnO nanoparticle. Synth React Inorg, Met-Org, Nano-Met Chem 43:406–411
48. Addison AW, Rao TN, Reedijk J, van Rijn J, Verschoor GC (1984) Synthesis, structure, and spectroscopic properties of copper (II) compounds containing nitrogen–sulphur donor ligands; the crystal and molecular structure of aqua [1, 7-bis (*N*-methylbenzimidazol-2′-yl)-2, 6-dithiaheptane] copper (II) perchlorate. J Chem Soc Dalton Trans 1349–1356
49. Tobón-Trujillo LM, Villanueva-Sánchez LF, Martínez-Otero D, Dorazco-González A (2015) Crystal structure of bis (μ2-tetrabromophthalato-κ2O1: O2) bis [aqua (N, N, N′, N′-tetramethylethane-1, 2-diamine-κ2 N, N′) copper (II)]. Acta Crystallogr Sect E Crystallogr Commun 71:m171–m172
50. Arjmand F, Mohani B, Ahmad S (2005) Synthesis, antibacterial, antifungal activity and interaction of CT-DNA with a new benzimidazole derived Cu (II) complex. Eur J Med Chem 40:1103–1110
51. Szczepanik W, Ciesiołka J, Wrzesiński J, Skała J, Jeżowska-Bojczuk M (2003) Interaction of aminoglycosides and their copper(ii) complexes with nucleic acids: implication to the toxicity of these drugs. Dalton Trans 1488–1494
52. Arjmand F, Sayeed F, Parveen S, Tabassum S, Juvekar AS, Zingde SM (2013) Design and synthesis of (*S*)- and (*R*)-enantiomers of [4-(2-hydroxy-1-phenylethylimino) pent-2-ol] dimethyltin (IV) and 2, 2-dimethyl-4-phenyl-1, 3, 2-oxazastannolidine: in vitro antitumor activity against human tumor cell lines and in vivo assay of (*S*)-enantiomers. Dalton Trans 42:3390–3401
53. Alizadeh R, Afzal M, Arjmand F (2014) In vitro DNA binding, pBR322 plasmid cleavage and molecular modeling study of chiral benzothiazole Schiff-base-valine Cu (II) and Zn (II) complexes to evaluate their enantiomeric biological disposition for molecular target DNA. Spectrochim Acta Part A Mol Biomol Spectrosc 131:625–635
54. Sudhamani CN, Naik HSB, Naik TRR, Prabhakara MC (2009) Synthesis, DNA binding and cleavage studies of Ni(II) complexes with fused aromatic N-containing ligands. Spectrochim Acta Part A Mol Biomol Spectrosc 72:643–647
55. Zhang G, Fu P, Wang L, Hu M (2011) Molecular spectroscopic studies of farrerol interaction with Calf Thymus DNA. J Agric Food Chem 59:8944–8952
56. Akdi K, Vilaplana RA, Kamah S, González-Vílchez F (2005) Effects of Tris and Hepes buffers on the interaction of palladium–diaminopropane complexes with DNA. J Inorg Biochem 99:1360–1368
57. Shahabadi N, Kashanian S, Fatahi A (2011) Identification of binding mode of a platinum (II) complex, PtCl(2)(DIP), and Calf Thymus DNA. Bioinorg Chem Appl 2011:687571
58. Li Q, Yang P, Wang H, Guo M (1996) Diorganotin(IV) antitumor agent. (C2H5)2SnCl2 (phen)/nucleotides aqueous and solid-state coordination chemistry and its DNA binding studies. J Inorg Biochem 64:181–195
59. Shi S, Liu J, Li J, Zheng KC, Huang XM, Tan CP, Chen LM, Ji LN (2006) Synthesis, characterization and DNA-binding of novel chiral complexes delta- and lambda-[Ru(bpy)2L]2 + (L = o-mopip and p-mopip). J Inorg Biochem 100:385–395
60. Jaumot J, Gargallo R (2012) Experimental methods for studying the interactions between G-quadruplex structures and ligands. Curr Pharm Des 18:1900–1916
61. Sun H, Xiang J, Liu Y, Li L, Li Q, Xu G, Tang Y (2011) A stabilizing and denaturing dual-effect for natural polyamines interacting with G-quadruplexes depending on concentration. Biochimie 93:1351–1356
62. Arjmand F, Parveen S, Afzal M, Toupet L, Hadda TB (2012) Molecular drug design, synthesis and crystal structure determination of Cu II–Sn IV heterobimetallic core: DNA binding and cleavage studies. Eur J Med Chem 49:141–150
63. Lazic D, Arsenijevic A, Puchta R, Bugarcic ZD, Rilak A (2016) DNA binding properties, histidine interaction and cytotoxicity studies of water soluble ruthenium(ii) terpyridine complexes. Dalton Trans (Cambridge, England: 2003) 45:4633–4646
64. Milutinović MM, Bugarčić ŽD, Wilhelm R (2018) A camphor based 1,3-diamine Ru(ii) terpyridine complex: synthesis, characterization, kinetic investigation and DNA binding. New J Chem 42:7607–7611
65. Tabassum S, Zaki M, Afzal M, Arjmand F (2014) Synthesis and characterization of Cu(II)-based anticancer chemotherapeutic agent targeting topoisomerase Iα: in vitro DNA binding, pBR322 cleavage, molecular docking studies and cytotoxicity against human cancer cell lines. Eur J Med Chem 74:509–523
66. Liang F, Wang P, Zhou X, Li T, Li Z, Lin H, Gao D, Zheng C, Wu C (2004) Nickel(II) and cobalt(II) complexes of

hydroxyl-substituted triazamacrocyclic ligand as potential antitumor agents. Bioorg Med Chem Lett 14:1901–1904
67. Melvin MS, Tomlinson JT, Saluta GR, Kucera GL, Lindquist N, Manderville RA (2000) Double-Strand DNA Cleavage by Copper Prodigiosin. J Am Chem Soc 122:6333–6334
68. Arjmand F, Sharma GC, Muddassir M, Tabassum S (2011) Synthesis and enantiopreferential DNA-binding profile of late 3d transition metal R-and S-enantiomeric complexes derived from *N*, *N*-bis-(1-benzyl-2-ethoxyethane): validation of R-enantiomer of copper (II) complex as a human topoisomerase II inhibitor. Chirality 23:557–567
69. Tabassum S, Ahmad M, Afzal M, Zaki M, Bharadwaj PK (2014) Synthesis and structure elucidation of a copper(II) Schiff-base complex: in vitro DNA binding, pBR322 plasmid cleavage and HSA binding studies. J Photochem Photobiol B 140:321–331
70. Deng J, Su G, Chen P, Du Y, Gou Y, Liu Y (2018) Evaluation of DNA binding and DNA cleavage of nickel(II) complexes with tridentate α-N-heterocyclic thiosemicarbazones ligands. Inorg Chim Acta 471:194–202
71. Fu XB, Liu DD, Lin Y, Hu W, Mao ZW, Le XY (2014) Water-soluble DNA minor groove binders as potential chemotherapeutic agents: synthesis, characterization, DNA binding and cleavage, antioxidation, cytotoxicity and HSA interactions. Dalton Trans (Cambridge, England: 2003) 43:8721–8737
72. Alizadeh R, Yousuf I, Afzal M, Srivastav S, Srikrishna S, Arjmand F (2015) Enantiomeric fluoro-substituted benzothiazole Schiff base-valine Cu (II)/Zn (II) complexes as chemotherapeutic agents: DNA binding profile, cleavage activity, MTT assay and cell imaging studies. J Photochem Photobiol B 143:61–73
73. Kumari R, Nath M (2017) Tri- and diorganotin(IV) derivatives of non-steroidal anti-inflammatory drug sulindac: characterization, electronic structures (DFT), DNA binding and plasmid cleavage studies. Appl Organomet Chem 31:e3661
74. Annaraj B, Balakrishnan C, Neelakantan MA (2016) Synthesis, structure information, DNA/BSA binding affinity and in vitro cytotoxic studies of mixed ligand copper(II) complexes containing a phenylalanine derivative and diimine co-ligands. J Photochem Photobiol, B 160:278–291
75. Manan MAFA, Tahir MIM, Crouse KA, Rosli R, How FN-F, Watkin DJ (2011) The crystal structure and cytotoxicity of centrosymmetric copper(II) complex derived from *S*-methyldithiocarbazate with Isatin. J Chem Crystallogr 41:1866–1871
76. Sriwiriyajan S, Ninpesh T, Sukpondma Y, Nasomyon T, Graidist P (2014) Cytotoxicity screening of plants of genus piper in breast cancer cell lines. Trop J Pharmaceut Res 13:921–928
77. Gren R (1972) Protocol for screening chemical agents and natural product against animal tumors and other biological system. Cancer Chemother Rep 3:51–61

Affiliations

Büşra Kaya[1] · Zehra Kübra Yılmaz[2] · Onur Şahin[3] · Belma Aslim[2] · Ümmügülsüm Tükenmez[4] · Bahri Ülküseven[1]

✉ Bahri Ülküseven
bahseven@istanbul.edu.tr

[1] Department of Chemistry, Engineering Faculty, Istanbul University-Cerrahpasa, Avcilar, 34320 Istanbul, Turkey

[2] Faculty of Science, Department of Biology, Gazi University, Ankara, Turkey

[3] Scientific and Technological Research Application and Research Center, Sinop University, 57000 Sinop, Turkey

[4] Vocational High School of Health Services, Mardin Artuklu University, Mardin, Turkey